Appearance Acquisition and Analysis of Effect Coatings

Jiří Filip[a], Frank J. Maile[b]

[a]*Institute of Information Theory and Automation of the CAS, Prague, Czech Republic*
[b]*Schlenk Metallic Pigments, GmbH, Roth, Germany*

Abstract

Effect coatings capturing, visualization and analysis become highly important nowadays, when digital appearance content is necessary for facilitating quick communication of material appearance properties across various industries. This paper briefly overviews our recent contributions to: (1) rapid and realistic appearance measurement and visualization of effect coatings, (2) characterization of effect coatings allowing instant discrimination between different coating systems and effect pigments, (3) a non-invasive automatic texture-based particle orientation analysis method.

Keywords: effect coatings, appearance capturing, polychromatic, particle orientation

1. Introduction

The high fidelity appearance reproduction of coating or plastic materials containing effect pigments allow the acceleration of product design cycles. Therefore, a proper and reliable characterization of these surfaces containing different effect pigments [1] like metallics, pearls or polychromatics is of high interest for designers as well as to the complete coatings and plastics industry, especially when it comes to quality control.

The paper is organized as follows. Section 2 describes the appearance capturing approach. Section 3 introduces test materials which are used for further analysis. Section 4 demonstrates the ability of the image-based method in order to characterize different coating systems and materials. Finally, Section 5 proposes a novel approach to particle orientation analysis.

2. Effect coatings appearance capture

2.1. Capturing devices

We captured coatings appearance using two devices [2] as shown in Fig. 1.

The reference UTIA gonioreflectometer (on the left) features 4 mechanical degrees of freedom. This state-of-the-art setup [3] consists of the measured sample held by a rotating stage and two independently controlled arms with camera (one axis) and light (two axes). It allows for flexible and adaptive measurements of nearly arbitrary combinations of illumination and viewing directions. Although camera view occlusion by arm with light may occur, it can be analytically detected, and in most cases alternative positioning is possible. Verified illumination and camera arms positioning angular accuracy across all axes is 0.03^o. The inner arm holds LED light source 1.1m from sample producing a narrow and uniform beam of light. The outer arm holds an industrial full-frame 16Mpix RGB camera AVT Pike 1600C. The sensor's distance from the sample is 2m. Using different optics we can achieved spatial resolution up to 1071 DPI (i.e., 24 μm/pixel), which constrained maximal sample's size to 44x44 mm. Samples of size up to 139x139 mm can be measured in a resolution of 350 DPI.

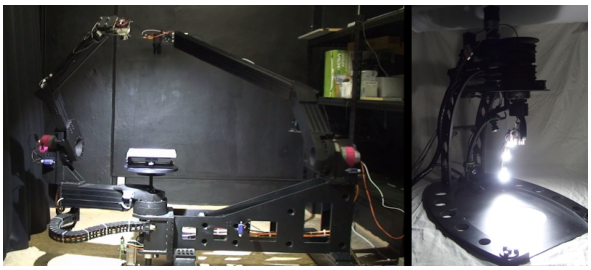

Figure 1: Gonioreflectometers used for capturing of material appearance at UTIA: (left) the reference, (right) its portable counterpart for rapid appearance acquisition.

A portable gonioreflectometer is an automatic appearance capturing device based on a concept of two

Email addresses: filipj@utia.cas.cz (Jiří Filip), frank.maile@schlenk.de (Frank J. Maile)

URL: http://staff.utia.cas.cz/filip (Jiří Filip), http://www.schlenk.de (Frank J. Maile)

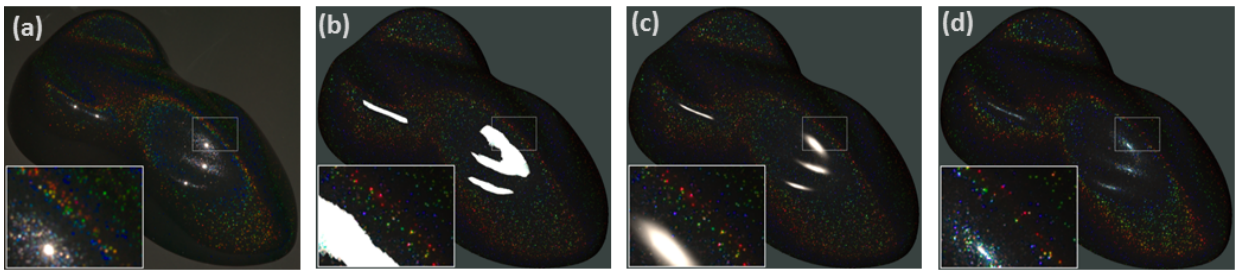

Figure 2: Side-by-side comparison of a real shape photograph (a) with the respective material rendering using a BTF (b), BTF combined with the Fresnel model of specular highlights (c), and using the bivariate representation (d).

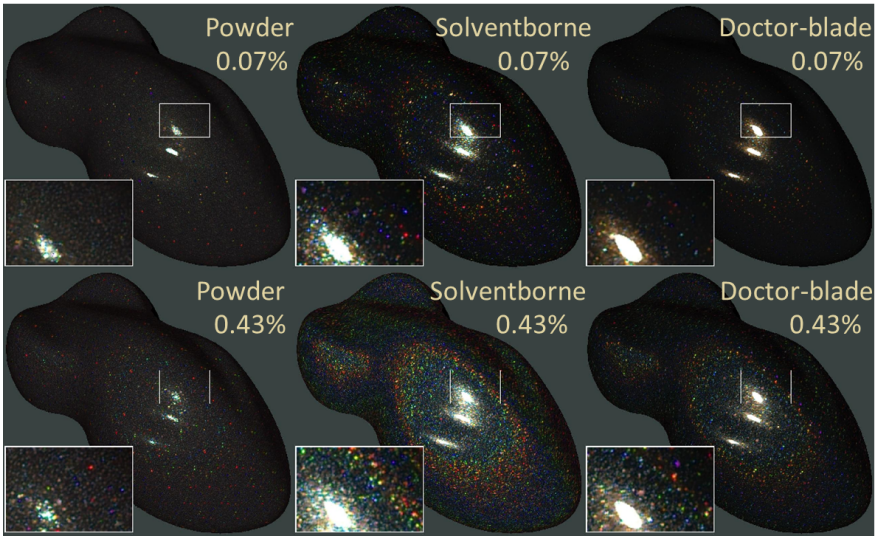

Figure 3: The sample set 1 featuring different pigment concentrations (rows) and coating systems (columns).

independent arms holding three LED lights and three RGB cameras of a resolution of 1.3Mpix. It captures sample of size up to 3x3cm with a resolution of 400DPI. Setup's automatic calibration, movement of the arms, and capturing of images is controlled remotely from a PC with a typical measurement time of 20 minutes. The device captures HDR data mutually registered at sub-pixel accuracy. The setup is portable of weight 20kg and thus can also be used for field measurements. Due to a modular concept of the device, one can use up to six lights and cameras and thus adapt the speed of measurement procedure and captured data fidelity to application needs.

2.2. Appearance representations

Depending on application, several approaches to material appearance representation exist [4]. A common way of representing material apparance is using a *bidirectional reflectance distribution function* (BRDF) [5] describing the distribution of energy reflected in the viewing direction when illuminated from a specific direction. As the BRDF itself cannot capture a material's spatial structure, it has been extended to a more general *bidirectional texture function* (BTF) [6] capturing non-local effects in rough material structures, such as occlusions, masking, sub-surface scattering, or inter-reflections. A monospectral BTF is a six-dimensional function representing the material appearance at each surface point for variable illumination and view directions, parameterized by elevation and azimuthal angles. As the BTF data achieves photo-realistic visualization of material appearance it has high application potential also in the effect coatings industry.

We typically capture BTF data using 81 illumination and 81 viewing directions over a hemisphere resulting in 6561 captured HDR images of the material. Unfortunately, even such high number of images is unable to correctly characterize the area near the specular highlight as is show in Fig. 2-b (material featuring a MultiFlect©) polychromatic effect with a clear coat layer). The material was rendered on a 3D object so we could compare the captured appearance to a photo of a

real coated shape using the same pigment Fig. 2-a. One can see a significant difference especially near specular highlight where low sampling in inclinations (15^o) results in energy leakage to the surrounding directions due to data interpolation in an angular domain. One way to avoid this artifact is removing the specular samples and substitute them by the Fresnel model of specular highlights. Although this modelling improves the highlight appearance (Fig. 2-c), it is still far from being accurate as the parameters of the model cannot be properly established without taking additional image samples. Our solution relies on the assumptions valid for the effect coatings, i.e., azimuthal isotropy and bilateral symmetry. Therefore, we transform the illumination and viewing directions to the half-vector parametrization [7] and use the assumptions to neglect two of its four angular dimensions. The resulting bivariate texture representation allows much better characterization of specular highlights Fig. 2-d than the BTF-based approaches. Moreover, while the capturing of BTF took, due to mechanical positioning, exposure and data transfer of 6561 HDR image samples typically take around 20 hours, the 102 images needed by the bivariate representation are recorded in less than 20 minutes.

3. Test coating samples

In the following two sections we optically analyzed two sets of effect coatings samples.

The first of them is shown in Fig. 3. It consists of six samples using polychromatic effect pigment (MultiFlect®), three of them with the pigment concentration 0.07% (the first row) and three with the concentration 0.43% (the second row). Further, the samples in each row differ in a type of coating system used for identical pigment application. From left to right we used: (1) powder-coating, (2) a solventborne system, (3) the solventborne applied using a doctor-blade.

The second test set combines samples using different types of flakes and different substrates. Samples M1–M4 feature polychromatic pigment (MultiFlect®), sample M5 and M6 feature aluminum pigment, and samples M7 and M8 uses white mica effect pigments.

4. Characterization of effect coatings

4.1. Light diffraction theory

Interference pigments are employed in many automotive and industrial paint formulations. The principle behind their appearance is driven by by physics of light diffraction on a regular grating of spacing comparable to wavelength of incident light. The grating is a collection of reflecting elements introduced either by regular ruling or by means of lithographic methods. Fig. 5 depicts a grating foil, which is the precursor for the polychromatic effect pigment used in a coating layer or plastic material in order to achieve an attractive appearance of object.

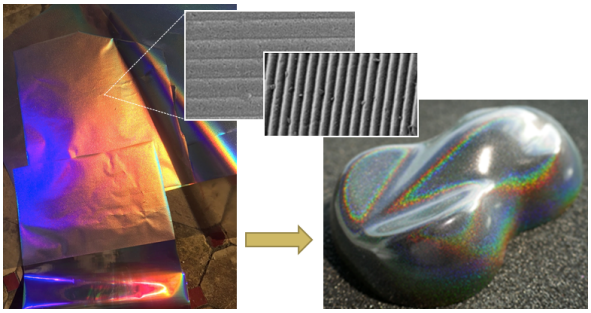

Figure 5: The grating foil, a precursor for manufacturing of polychromatic effect pigment (left). A microscopy image showing a detail of the grating (top). Appearance of an object after coating application of particles made from a grating foil (right).

The basic principle is explained on a simplified example of in-plane geometry in Fig. 6, where incident light from elevation angle α reflects from the grating with a groove spacing d and is observed in elevation angle β [8]. These relations are expressed by the principal grating equation

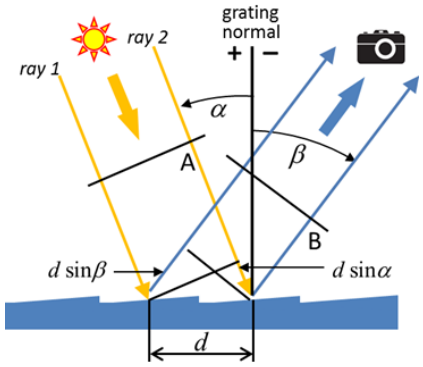

Figure 6: A scheme showing a basic principle of light diffraction on the regular grating within in-plane geometry.

$$m\lambda = d(\sin\alpha + \sin\beta) \ , \tag{1}$$

where m is a diffraction order, an integer value specifying order of interest, either negative or positive. The zero order $m = 0$ corresponds to specular reflection.

However, once we need to model complex appearance of object with polychromatic particles, we have to expand this equation by means of additional azimuthal

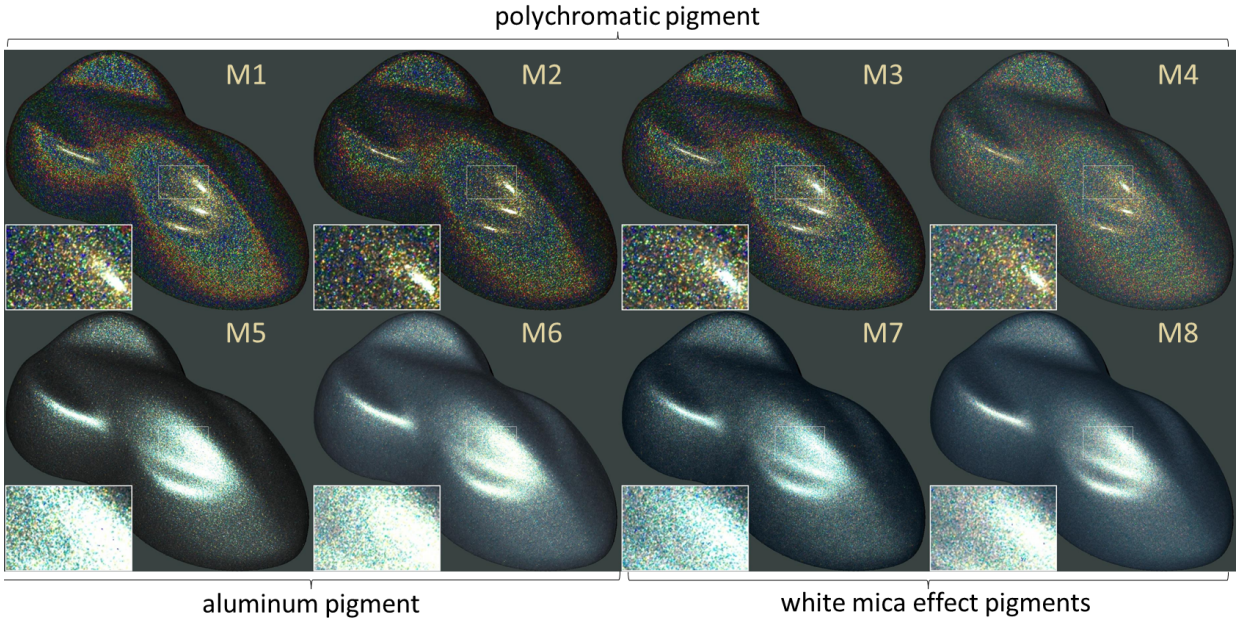

Figure 4: The sample set 2 featuring three types of effect pigments in combination with different substrate treatments.

terms. Thus the general grating equation can be derived as

$$m\lambda = \frac{d\,[t_3 + t_4]}{\sqrt{t_1^2 + t_2^2 + 2t_1 t_2 \cos(\varphi_i - \varphi_v)}} \tag{2}$$

$$t_1 = \tan\theta_v \qquad t_2 = \tan\theta_i \tag{3}$$

$$t_3 = [\sin\theta_i + \sin\theta_v \cos(\varphi_i - \varphi_v)]t_1 \tag{4}$$

$$t_4 = [\sin\theta_v + \sin\theta_i \cos(\varphi_i - \varphi_v)]t_2 \ , \tag{5}$$

where θ_i and θ_v are inclination angles of illumination and sensor, and φ_i and φ_v are respective azimuthal angles as shown in Fig. 7.

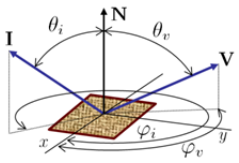

Figure 7: A parameterization of incoming and outgoing angles withing a material coordinate system.

Once the general diffraction model is established we can visualize the appearance of any object under any view and lighting conditions Fig. 8-top, for arbitrary grating step d used for grating production. Fig. 8-bottom compares the model's performance to photograph of the same speedshape object coated using polychromatic pigment, demonstrating a good color agreement.

The ability of such modelling represent a set of additional constrains for particle orientation analysis. Once we reduce the dimensionality of the capturing geometry we can even use the grating equation for a direct estimate of the particle distribution statistics.

4.2. Characterization of polychromatic coating systems

Once we limit our analysis to in-plane geometry only (camera at 45^o and moving light perpendicular to the grating), we obtain gonioapparent response for individual RGB channels of our camera as shown in graph in Fig. 9-top. The graph clearly distinguishes between individual diffraction orders, where 0-order represents a specular reflection. For demonstration purposes, we selected several images sampled across refraction orders 0-2 and compare appearance of polychromatic foil and two coatings systems (powder and solventborn) using the same polychromatic effect pigment produced from the foil Fig. 9-bottom.

One can immediately observe apparent visual differences between the systems. As the differences are related especially to the density and a number of effective pigment over a unit area, we developed an image processing method computing pigment count and pigment coverage area. The results of such analysis of sample set 1 for in-plane geometry are shown in Fig. 10. The graph on the left show the results for the lower pigmentation while graphs on the right show the same for the higher pigmentation. The first row depicts percentage,

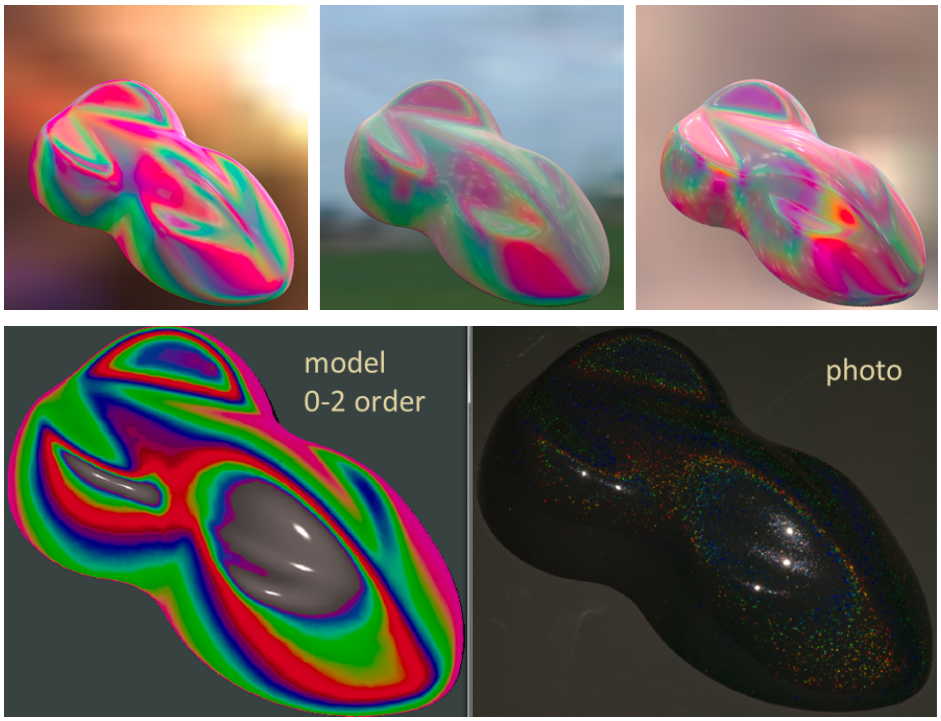

Figure 8: Top: An example of holographic foil appearance modelling visualized in different illumination environments. Bottom: The result of holographic behavior modelling compared to photograph of speed shape in identical viewing and lighting conditions.

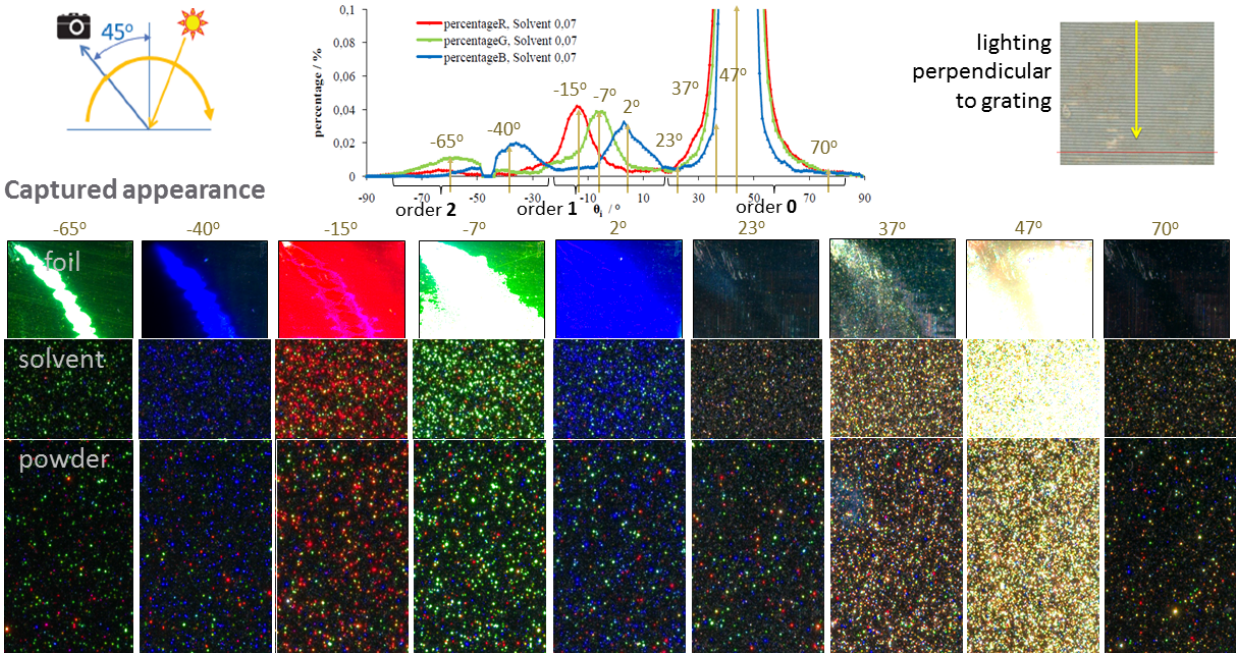

Figure 9: A comparison of selected images from in-plane geometry: a holographic foil and its application as a pigment using two coating systems - powder and solventborne.

the second one count of pigment, and the last one average pigment intensity. From the graph we can clearly tell differences between the coating systems (red: solventborne, green: powder, blue: the solventborne ap-

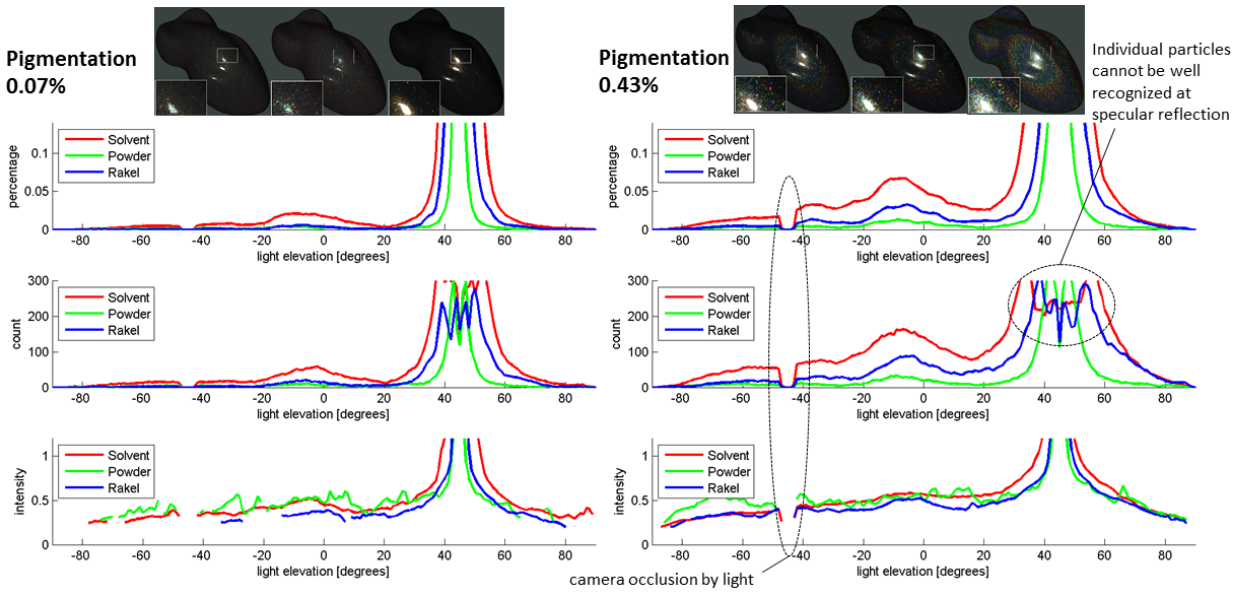

Figure 10: Results of discrimination between different coating systems within in-plane geometry (red: solventborne, green: powder, blue: the solventborne applied using a doctor blade denoted as Rakel) for two pigment concentrations (columns). The first row compares the area coverage by the pigment in %, the second row compares particles counts, and the third row compares average pigment intensity.

plied using a doctor-blade denoted as Rakel) and pigment concentrations across the inclination angles. In the right graph one can spot limitations of the method: (1) intensity drop near 45^o due to the camera occlusion by the light, (2) noise within specular-peak area of particles count graph, where the method cannot reliably distinguish between flake and clear-coat reflection.

The same analysis can be performed for out-of-plane geometry (both light and camera inclinations 45^o, light azimuth change) as shown in Fig. 11. The color graph on the left shows pigment count while the graph on the right shows its coverage in %. Again we can see a clear discrimination between three coating systems.

4.3. Characterization of flake materials

Similarly to different coating systems we can apply our method to the analysis of different effect pigment materials represented by sample set 2. Results of the out-of-plane analysis are shown in Fig. 12. Here we can see a clear differentiation between polychromatic and non-polychromatic pigments, where the former exhibit characteristic high-order highlights when compared to aluminum and white mica effect pigments.

4.4. Characterization of clear-coat properties

Finally, we show that our method allows successfully to analyze also the impact of clear-coat as illustrated in Fig. 13 on example analysis of MultiFlect© effect pigment with and without the clear-coat layer.

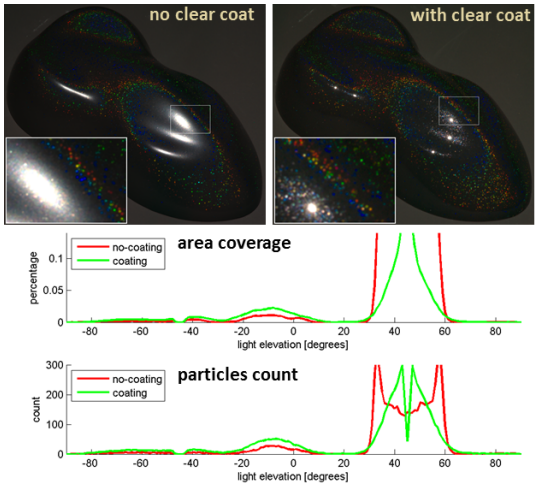

Figure 13: An analysis of clear-coat presence impact within an in-plane geometry.

5. Particle orientation analysis in effect coatings

In the last part of this report we introduce a novel image-based method for particle orientation analysis in effect coatings. Particle orientation is, among others, particularly important especially for understanding the influence of multiple parameters on fine particle orientation in the entire coating application process [1], hence quality control is nowadays typically obtained by semi-automatic analysis of sample cross-cuts in microscopy images (see Fig. 14 and Fig. 15-right) [9]. Such an anal-

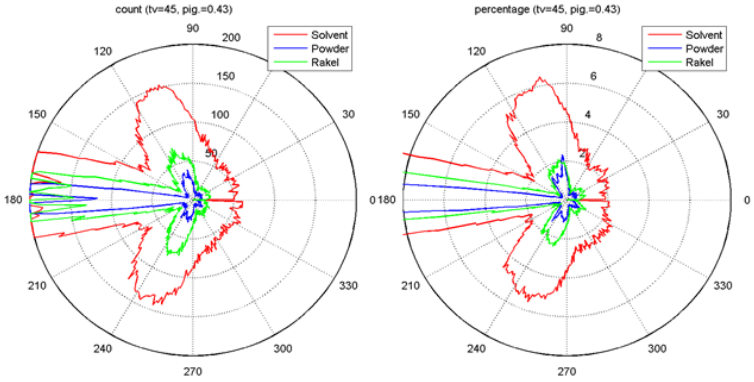

Figure 11: Results of the discrimination between different coating systems in out-of-plane geometry (red: solventborne, green: powder, blue: the solventborne applied using a doctor blade denoted as Rakel) for the pigment concentration 0.43%: (left) pigment count, (right) pigment coverage.

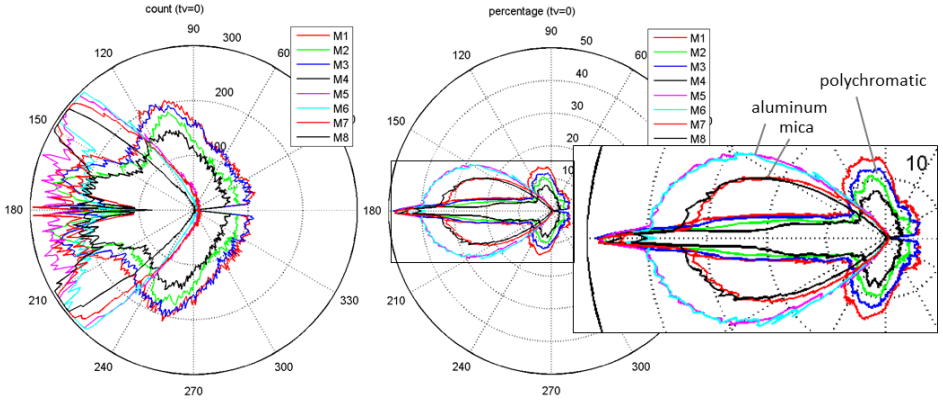

Figure 12: Results of a discrimination between flake materials in out-of-plane geometry: (left) pigment count, (right) pigment coverage.

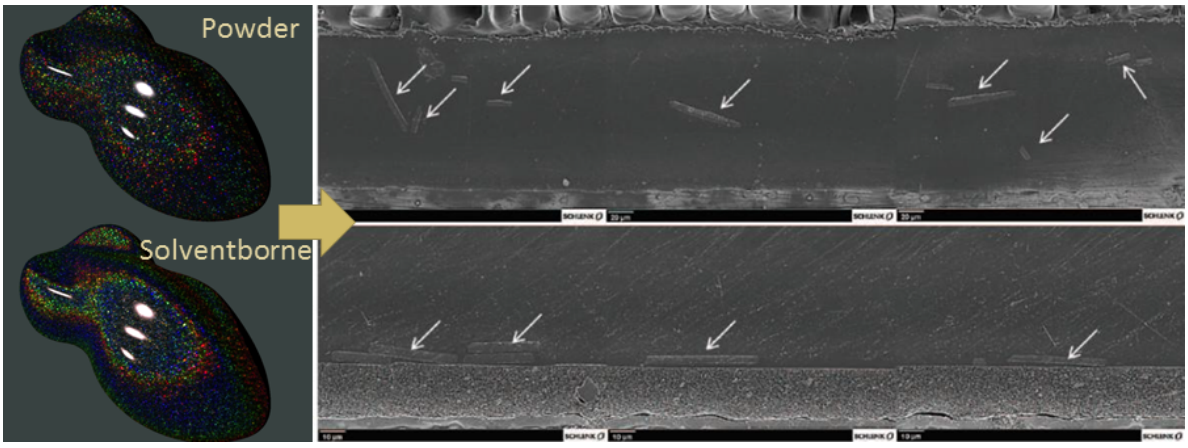

Figure 15: A visual comparison of two coating systems captured appearance and corresponding images from scanning electron microscopy.

ysis is considerably time and resources demanding as it requires specific preparation of the samples and relies on human observers within the analytic process. Therefore, our motivation is the development of an automatic solution allowing a non-invasive analysis of particle orientation. Our captured data visualizations and analysis in the previous sections revealed, that a texture-based approach can help automatically to distinguish between even very subtle differences in effect coatings (Fig. 15-left), therefore, we build on this analysis and extend its abilities to particle orientation estimation.

The basic idea of our method, outlined in Fig. 16,

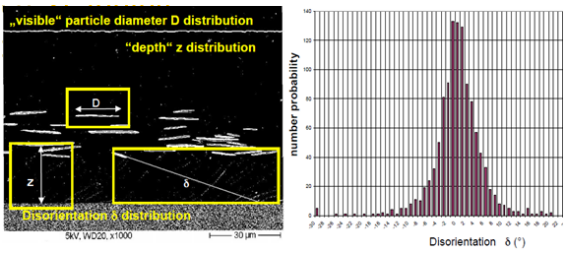

Figure 14: An example of particle inclination distribution as obtained from microscopic image of the sample cross-cut. Courtesy of [9].

assumes that each flake acts as an ideal mirror. When we have a control over light and sensor positioning we know the position of half-way vector **H**. The flake exhibits a strong reflection when the vector **H** is close to a normal vector of the flake. Therefore, if we sample a sufficient number of illumination directions we increase a probability of finding the close to normal vector. To this end, we capture almost thousand of illumination directions by means of multiple passes of light over the hemisphere at 14 different elevations. This gen-

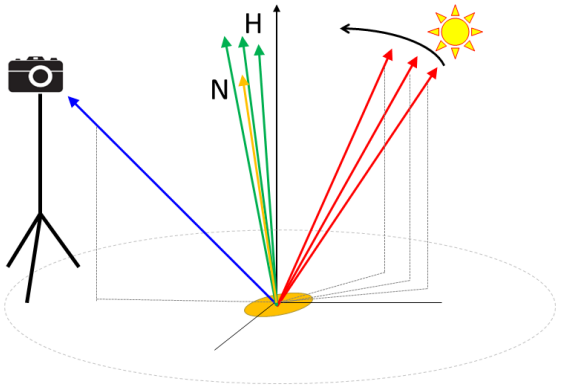

Figure 16: A principle of the proposed particle orientation analysis approach.

eral principle is valid for all mirror-like acting flakes except polychromatic MultiFlect© pigments . For those we have to distinguish between zero and higher reflection highlights as the higher orders could compromise our method's performance. To resolve this, we compare intensities of individual RGB channels and count only the normal candidates that have relatively close values, i.e. corresponding to zero-order diffraction.

An overview of geometry configuration used in our experiment is shown in Fig. 17, where the red dots represent light positions and the green dots corresponding tested normal candidates. The camera position was at inclination 45^o and light inclinations ranged between 30-60^o.

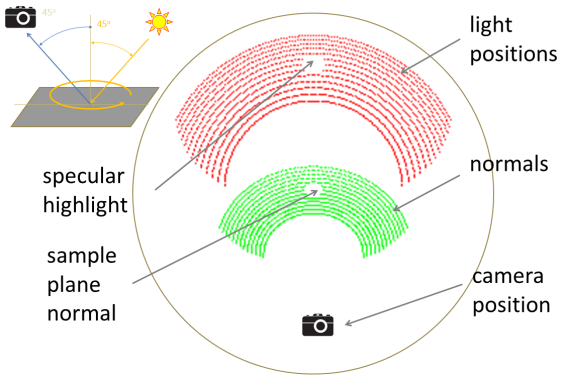

Figure 17: A geometry configuration used for the particle orientation analysis.

A block scheme in Fig. 18 illustrates the data analysis process. First, a per-pixel map of maximal intensities across all illuminations is obtained. Here we have to select only those having close-to-mirror reflection, i.e. with the highest value. We use a threshold related to multiple of median value of the per-pixel map. From the selected candidate pixels we can compute: (1) a particle distribution statistics and (2) particle orientation distribution function.

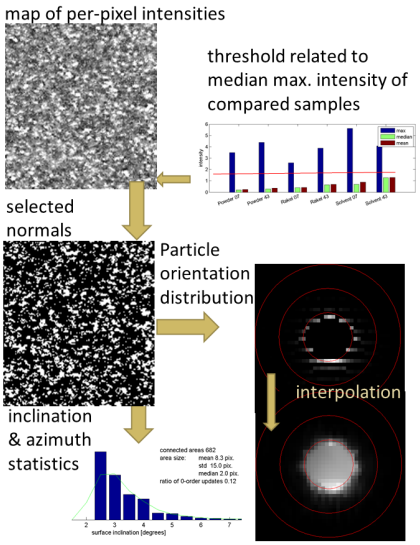

Figure 18: A block scheme of the proposed particle orientation analysis method.

The particle inclination histograms obtained by the proposed method for both test sample sets are shown in Fig. 19. The first row show absolute values while the second row show graphs normalized according to the maximal values. One can clearly distinguish between the samples. The left graph show clear differentiation between powder and other coating systems. Also

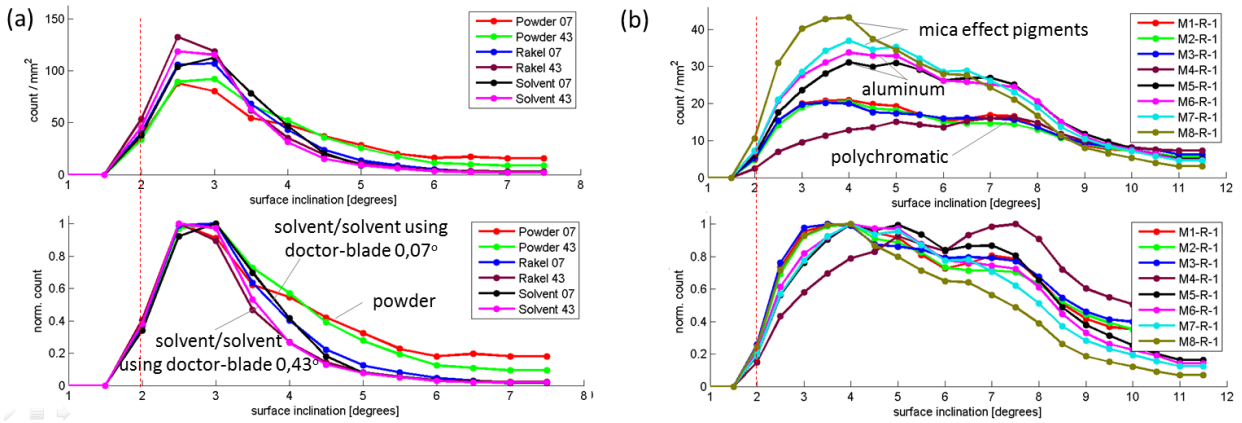

Figure 19: Histograms of particle inclination (a) for the sample set 1, (b) for the sample set 2. The second row shows histograms normalized according to their maximal values. The dashed outline depicts a boundary of the evaluated inclinations.

show a difference between samples with different pigment concentrations. Note that near specular highlight we cannot optically distinguish between reflection from flakes and clear-coat. This is the reason for the drop of histogram values near inclination 0^o degrees as we had to restrict a proximity of tested illumination direction to 4^o from a specular highlight, which translates to a maximum of 2^o proximity of tested normals to the sample surface normal.

Finally, we can view the obtained data from a different perspective as is shown in Fig. 20. We can record illumination-dependent gonioapparent behavior (or reflectance field) of each pixel. The Fig. 20 show for each sample location of the observed pixel, its illumination-dependent RGB map, and thresholded image useful for counting of candidate particles count and analysis of their orientation. For lower pigment concentrations we can see none or one highlight in such a RGB pixelmap, however, for higher pigmentations (sample set 2) we can clearly find more specular peaks. Those peaks are related to a number of particles covered by the particular pixel or by superposition of their intensities. This approach allows overcoming a limited resolution of imaging sensor and reveal the underlying behavior of particles under a single pixel.

Fig. 21 shows average numbers of specular peaks across 150 pixels for all tested samples. From the results one can observe significant differences between both sample sets. The differences are related especially to coating systems and pigment concentrations. In the future work we plan to extend this analysis by analytical differentiation of specular highlight from peaks caused due to superposition of higher diffraction order of polychromatic effect flakes. Although the method has some limitations arising from its optical principle we consider it as a promising tool for rapid non-invasive particle orientation analysis.

6. Conclusions

The main contributions of this report are:

- An overview on UTIA current abilities to capture appearance of effect coatings.
- A novel image-based approach to characterization of effect pigments capable of distinguishing between different coating systems (powder / solvent-borne / doctor blade), and between different effect pigment (polychromatic / aluminum / mica).
- A novel image-based approach to rapid non-invasive particle orientation analysis.

Acknowledgments

We would like to thank Bill Eibon (PPG) for inspiring discussions and preparation of coatings samples, Theresa Hartel (Schlenk) for additional analysis of polychromatic data samples, Radomír Vávra and Prof. Michal Haindl (UTIA CAS, v.v.i.) for help with data capturing and overall support.

This research has been supported by the Czech Science Foundation grant GA17-18407S (*Perceptually Optimized Measurement of Material Appearance*).

7. References

[1] F. J. Maile, G. Pfaff, P. Reynders, Effect pigment – past, present and future, Progress in Organic Coatings 54 (3) (2005) 150 – 163.

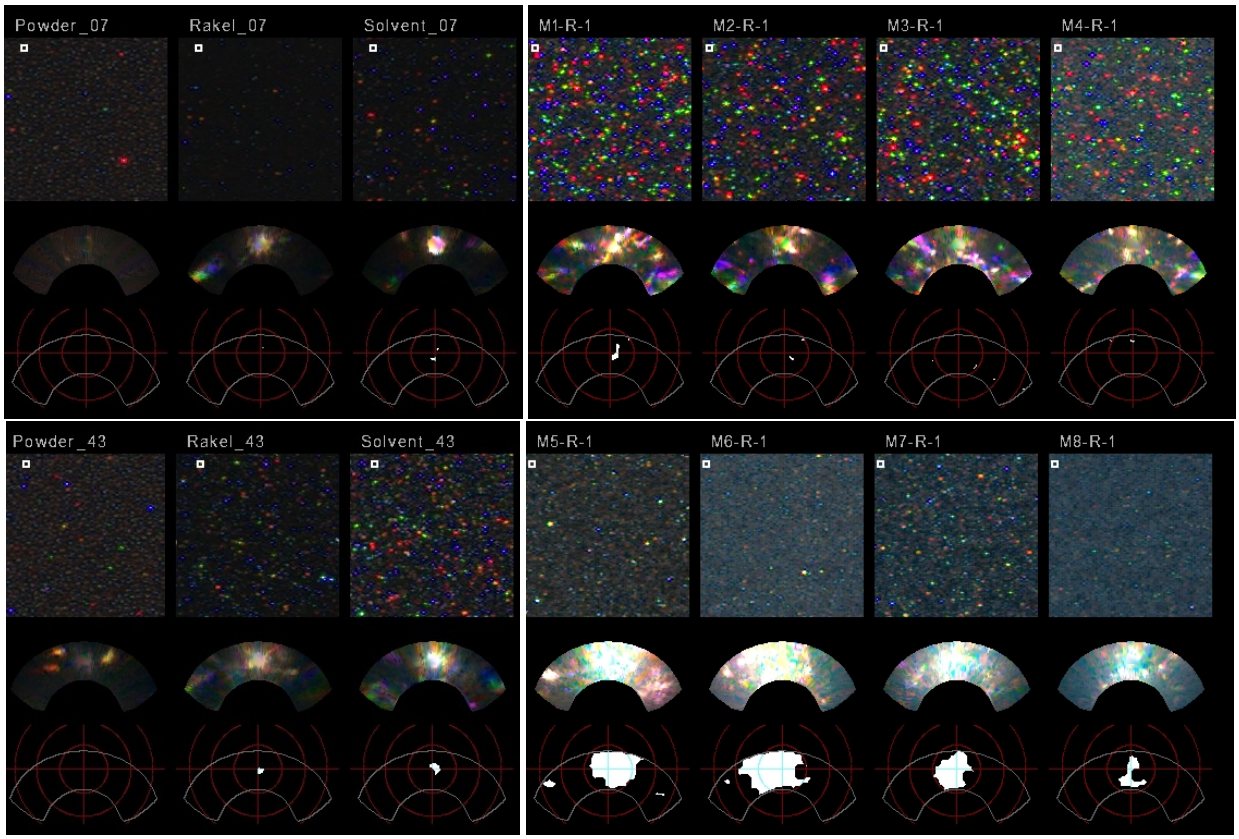

Figure 20: An example of behavior of a selected pixel for all tested samples. For each pixel (highlighted by white square) its illumination-dependent appearance is plotted together with a thresholded image showing candidates of particles orientations. The red circles depict 10^o steps in inclinations, their center points to top of a hemisphere.

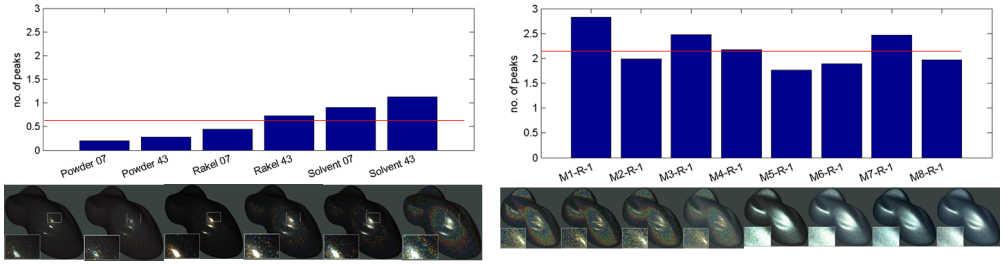

Figure 21: Average number of specular peaks computed by thresholding of illumination-dependent pixelmaps: (left) results for sample set 1, (right) results for sample sat 2. The red outline show an average number of peaks per pixel.

[2] J. Filip, R. Vavra, M. Haindl, Capturing material visualization data using goniometers, in: Proceedings of the 4th CIE Expert Symposium on Colour and Visual Appearance, Vol. CIE x043:2016, CIE, 2016, pp. 121–127.

[3] J. Filip, R. Vávra, M. Haindl, P. Zid, M. Krupicka, V. Havran, BRDF slices: Accurate adaptive anisotropic appearance acquisition, in: In proceedings of the 26th IEEE Conference on Computer Vision and Pattern Recognition, CVPR 2013, 2013, pp. 4321–4326.

[4] M. Haindl, J. Filip, Visual Texture, Advances in Computer Vision and Pattern Recognition, Springer-Verlag, London, 2013.

[5] F. Nicodemus, J. Richmond, J. Hsia, I. Ginsburg, T. Limperis, Geometrical considerations and nomenclature for reflectance, NBS Monograph 160 (1977) 1–52.

[6] K. Dana, B. van Ginneken, S. Nayar, J. Koenderink, Reflectance and texture of real-world surfaces, ACM Transactions on Graphics 18 (1) (1999) 1–34.

[7] S. Rusinkiewicz, A new change of variables for efficient BRDF representation, in: Rendering techniques' 98, 1998, pp. 11–22.

[8] C. Palmer, E. Loewen, Diffraction Grating Handbook, Newport Corporation; 6th edition, 705 St. Paul Street, Rochester, New York 14605 USA, 2004.

[9] F. Maile, M. Rösler, P. Reynders, M. Entenmann, Orientation of transparent effect pigments and its influence on their appearance in polymer films, in: COSI, 2007, p. 57.